Testing the constant-temperature approach for the nuclear level density

N. Dinh Dang,[1,2,*] N. Quang Hung,[3,†] and L. T. Quynh Huong[3,4,†]

[1]*Quantum Hadron Physics Laboratory, RIKEN Nishina Center for Accelerator-Based Science, 2-1 Hirosawa, Wako City, 351-0198 Saitama, Japan*
[2]*Institute for Nuclear Science and Technique, Hanoi, Vietnam*
[3]*Institute of Fundamental and Applied Sciences, Duy Tan University, 3 Quang Trung, Da Nang, Vietnam*
[4]*Faculty of Physics and Engineering Physics, Viet Nam National University Ho Chi Minh City – University of Science, Ho Chi Minh City, Vietnam*

The nuclear temperature is calculated from the derivative of the logarithm of the level densities in $^{60\text{-}62}$Ni and $^{170\text{-}172}$Yb. The latter are obtained within a method, which includes exact pairing for the levels around the Fermi surface in combination with the independent particle model for the rest of the single-particle spectrum. It is found that the increase in this temperature is relatively slow up to the excitation energy $E^* = E_f^*$ so that, at $0 < E^* \leqslant E_f^*$, the level density can be described well by the constant-temperature model. The values of E_f^* are found to be 10 MeV for $^{170\text{-}172}$Yb and 20 MeV for $^{60\text{-}62}$Ni, that is much higher than the particle separation threshold. Within this energy interval, the constant temperature is found to be around 0.5 MeV for $^{170\text{-}172}$Yb, whereas for $^{60\text{-}62}$Ni it can be any value between 1.3 and 1.5 MeV, in excellent agreement with the recent experimental finding. It is also shown that pairing plays an important role in maintaining this constant temperature at low excitation energy.

I. INTRODUCTION

The nuclear level density (NLD), defined as the number of excited levels per unit of excitation energy E^*, increases exponentially with E^*. This outstanding feature of NLD has paved the way for studying the average properties of nuclei within the framework of thermodynamics, such as pairing correlations, nuclear temperature, entropy, heat capacity, etc. [1]. NLD has important contributions in the study of low-energy nuclear reactions as well as nuclear astrophysics [2,3].

According to thermodynamics, the nuclear temperature is a parameter, which is defined from the NLD $\rho(E)$ as

$$T = \left[\frac{\partial \ln \rho(E)}{\partial E} \right]^{-1}. \qquad (1)$$

In the first model for NLD, which was proposed 80 years ago by Bethe [4] based on Fermi gas and led to the fundamental phenomenological formulas for NLD, such as the back-shifted Fermi gas, the NLD $\rho(E)$ is described approximately as $\exp(2\sqrt{aE^*})$ with the level-density parameter a. The nuclear temperature T, defined from Eq. (1), is then proportional to the square root of the excitation energy E^*, viz. $T \simeq \sqrt{E^*/a}$. Therefore, the Fermi-gas model implies an increase in nuclear temperature T with excitation energy E^*. However this model fails to describe the NLD at low excitation energies below the particle separation threshold.

The constant-temperature (CT) model, suggested by Gilbert and Cameron in 1965 [5], assumes that the NLD at low excitation energies ($E^* \leqslant 10$ MeV) can be described by a constant-temperature T, namely,

$$\rho(E^*) = \frac{1}{T} e^{(E^* - E_0)/T} \equiv B(T) e^{E^*/T},$$
$$B(T) = [T e^{E_0/T}]^{-1}. \qquad (2)$$

This model has become increasingly popular in the study of NLD in recent years [6–9] where it has been suggested that its validity can be extended to much higher excitation energies up to E^* around 20 MeV for ^{60}Ni and ^{60}Co isotopes [6]. The physical mechanism of this extension has been proposed based on the first-order phase transition from a superfluid to an ideal gas of quasiparticles [9] where most of the energy is absorbed near the critical temperature of $T_c \simeq 0.57\Delta(0)$, which is predicted within the finite-temperature Bardeen-Cooper-Schrieffer (FTBCS) theory, with $\Delta(0)$ being the pairing gap at zero-temperature $T = 0$. On the other hand, a number of studies in the past four decades have shown that, in finite systems, such as nuclei, thermal fluctuations smooth out the sharp phase transition from the superfluid phase to the normal one so that the pairing gap $\Delta(T)$ does not collapse at T_c but monotonically decreases with increasing T [10–16]. This property of finite systems may put under question the concept based on the first-order phase transition for extending the CT model to the region far above the particle separation energy. In this situation, it is highly desirable to analyze the validity of this phenomenological model by using a microscopic model, which is able to describe the NLD at both low as well as resonance energies. In Ref. [17], by comparing the shell-model results with the standard phenomenological approaches, it has been proposed that the CT model reflects the general process of nuclear chaotic dynamics.

Recently a unified approach has been proposed to simultaneously describe both the NLD and the radiative strength

———
[*]dang@riken.jp
[†]nqhungdtu@gmail.com

function based on the solution of exact pairing (EP) problem in combination with the independent-particle model (IPM), which is referred to as EP + IPM hereafter [18]. In the present paper, we will use this approach to study the validity of the CT model in nickel $^{60-62}$Ni and ytterbium $^{170-172}$Yb isotopes.

The paper is organized as follows. The formalism of the EP + IPM is outlined in Sec. II. The results of the numerical calculations are analyzed in Sec. III. The paper is summarized in the last section where conclusions are drawn.

II. DESCRIPTION OF NUCLEAR LEVEL DENSITY WITHIN THE EP + IPM

The present formalism employs the pairing Hamiltonian,

$$H = \sum_k \epsilon_k (a_{+k}^\dagger a_{+k} + a_{-k}^\dagger a_{-k}) - G \sum_{kk'} a_{+k}^\dagger a_{-k}^\dagger a_{-k'} a_{+k'}, \quad (3)$$

which describes the motion of protons and neutrons within their mean fields and their interactions via the monopole pairing forces. The strength of the pairing interaction is given by a constant G, which is different for protons and neutrons. The notations $a_{\pm k}^\dagger (a_{\pm k})$ are the creation (annihilation) operators of a nucleon with angular momentum k (in the deformed basis), projection $m_{\pm k}$, and energy ϵ_k for the kth level from Ω single-particle levels. This Hamiltonian (3) is diagonalized at $T = 0$ to obtain the exact eigenvalues $\mathcal{E}_S$ with S being the total seniority, which is equal to $0, 2, \ldots, \Omega$ for a system with an even number of particles and $1, 3, \ldots, \Omega$ for a system with an odd number of particles [19]. The exact partition function is constructed within the canonical ensemble (CE) at $T \neq 0$ by using these eigenvalues as [16,18]

$$Z(T) = \sum_S 2^S e^{-\mathcal{E}_S/T}. \quad (4)$$

All the thermodynamic quantities, such as free-energy $\mathcal{F}$, total-energy $\mathcal{E}$, heat-capacity $\mathcal{C}$, and pairing gap Δ are calculated from the partition function $Z(T)$ as

$$\mathcal{F} = -T \ln Z(T), \quad \mathcal{S} = -\frac{\partial \mathcal{F}}{\partial T} = \frac{\mathcal{E}}{T} + \ln Z(T), \quad (5)$$

$$\mathcal{E} = \mathcal{F} + T\mathcal{S}, \quad \mathcal{C} = \frac{\partial \mathcal{E}}{\partial T}, \quad (6)$$

$$\Delta = \sqrt{-G\mathcal{E}_{\text{pair}}}, \quad \mathcal{E}_{\text{pair}} = \mathcal{E} - 2 \sum_k \left[\epsilon_k - \frac{G}{2} f_k \right] f_k, \quad (7)$$

where the single-particle occupation numbers f_k are calculated from the state-dependent occupation numbers f_k^S as

$$f_k = \frac{1}{Z(T)} \sum_S 2^S f_k^{(S)} e^{-\mathcal{E}_S/T}. \quad (8)$$

This formalism exactly conserves the particle number at zero and finite temperatures, and the exact pairing gap Δ does not vanish at $T = T_c$ as the FTBCS gap but monotonically decreases with increasing T, remaining finite even at T as high as 5 MeV [16,18].

In practical calculations the size of the matrix to be diagonalized cannot be too large. Therefore the exact solutions of the pairing Hamiltonian are obtained only within a truncated subspace of single-particle levels around the Fermi surface where pairing is significant. The partition function $\mathcal{Z}(T)$ of

the total system is then calculated following the prescription in Refs. [20,21] as

$$\ln \mathcal{Z}(T) = \ln Z'_{\text{tr}}(T) + \ln Z'_{\text{sp}}(T) - \ln Z'_{\text{tr sp}}(T), \quad (9)$$

where $Z'_{\text{tr}}(T) \equiv Z_{\text{tr}}(T) \exp(\mathcal{E}_0/T)$ denotes the partition function with respect to the ground-state energy $\mathcal{E}_0$ with $Z_{\text{tr}}(T)$ being the exact partition function (4) obtained in the truncated subspace. The functions $Z'_{\text{sp}}(T) \equiv Z_{\text{sp}}(T) \exp(\mathcal{E}_0/T)$ and $Z'_{\text{tr sp}}(T) \equiv Z_{\text{tr sp}}(T) \exp(\mathcal{E}_0/T)$ are calculated by using the IPM partition functions $Z_{\text{sp}}(T)$ and $Z_{\text{tr sp}}(T)$, which are obtained within the IPM [22] for the entire single-particle spectrum and the truncated one, respectively.

The NLD $\rho(E)$ is calculated as the inverse Laplace transform of the partition function (9) in the saddle-point approximation as

$$\rho(E) = \frac{\omega(E)}{\sqrt{2\pi}\sigma}, \quad (10)$$

with the density of state $\omega(E)$ defined as [23]

$$\omega(E) = \frac{e^{\mathcal{S}}}{T\sqrt{2\pi\mathcal{C}}}, \quad (11)$$

where the entropy $\mathcal{S}$ and the heat-capacity $\mathcal{C}$ are obtained from the partition function $\mathcal{Z}(T)$ (9) by using their corresponding expressions in Eqs. (5)–(7).

The spin cutoff parameter σ in Eq. (10) describes the width of the spin distribution. In an axially deformed nucleus, there are two spin cutoff parameters, which are associated with the moments of inertia perpendicular ($\mathcal{I}_\perp$) and parallel ($\mathcal{I}_\parallel$) to the nuclear symmetry axis, denoted as $\sigma_\perp = \mathcal{I}_\perp T/\hbar^2$ and $\sigma_\parallel = \mathcal{I}_\parallel T/\hbar^2$, respectively. Their empirical expressions, based on the limit of a rigid body with the same density distribution as of the nucleus, are given as [24,25]

$$\sigma_\perp^2 \approx 0.015 A^{5/3} T, \quad \sigma_\parallel = \sigma_\perp \sqrt{\frac{3 - 2\beta_2}{3 + \beta_2}}, \quad (12)$$

where A is the mass number and β_2 is the quadrupole deformation parameter.

As the pairing Hamiltonian (3) includes neither interactions of higher multipolarities, such as dipole, quadrupole, etc., nor the rotational degree of freedom, the increase in NLD owing to collective vibrational and rotational excitations is introduced in terms of the vibrational k_{vib} and rotational k_{rot} enhancement factors following the description in Refs. [25–27]. They are defined as the ratios between the "correct" NLD including all degrees of freedom and the NLD where the collective vibration and rotation, respectively, are absent. Their empirical formulas are given as [25,27]

$$k_{\text{vib}} = e^{0.0555 A^{2/3} T^{4/3}}, \quad k_{\text{rot}} = \frac{\sigma_\perp^2 - 1}{1 + e^{[(E - U_C)/D_C]}} + 1, \quad (13)$$

with $D_C = 1400 \beta_2^2 A^{-2/3}$ and $U_C = 120 \beta_2^2 A^{1/3}$. An alternative treatment of k_{vib} based on the generalized boson partition function has been reported within the Hartree-Fock-Bogoliubov plus combinatorial (HFBC) method in Ref. [28], which separates the coherent particle-hole (ph) configurations forming the collective phonons from the incoherent ones to avoid double counting. The distribution of k_{vib} predicted within this alternative treatment is quantitatively equivalent to the
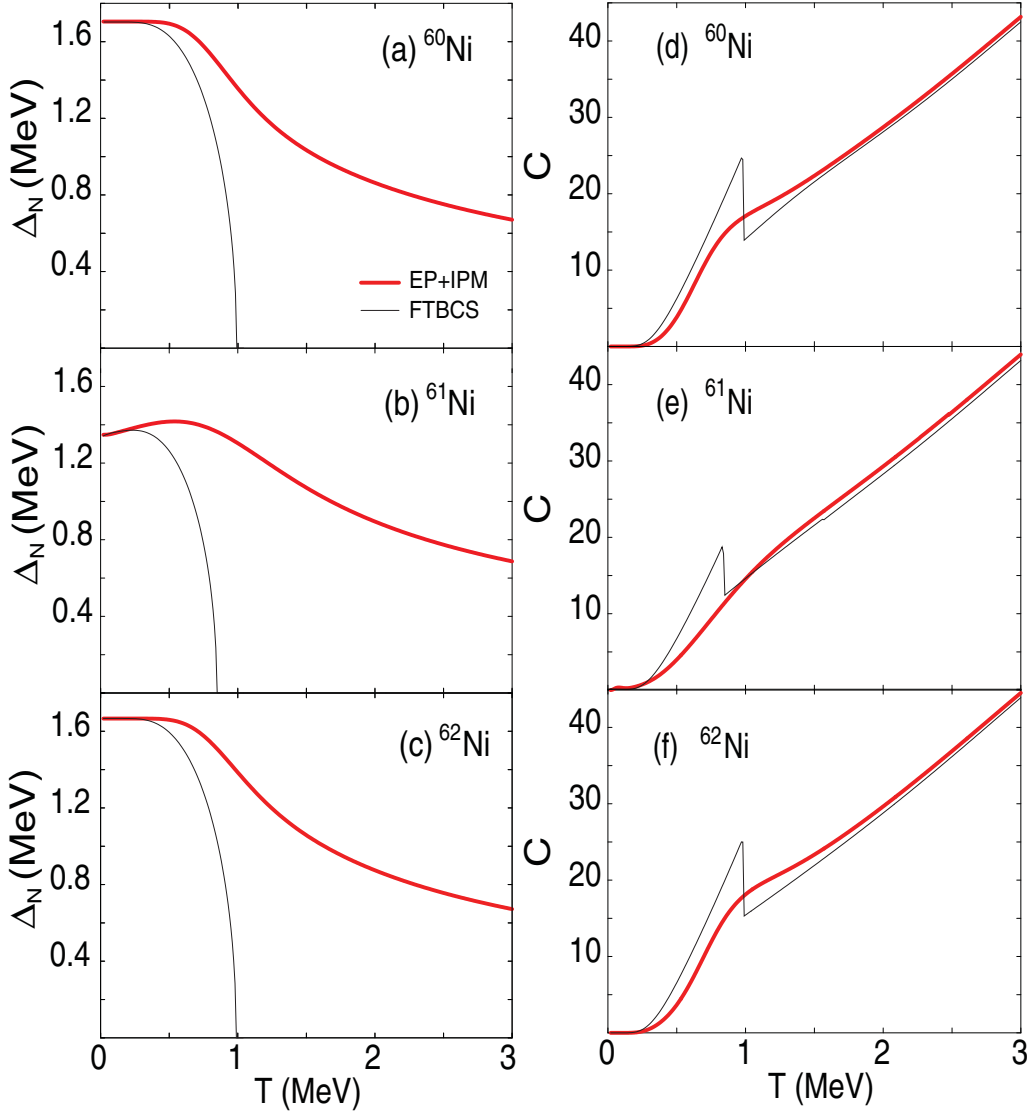
FIG. 1. Neutron pairing gaps Δ [(a)–(c)] and total heat-capacities C [(d)–(f)] as functions of T obtained within the EP + IPM (the thick solid line) and the FTBCS (the thin solid line) for $^{60-62}$Ni isotopes.

above-mentioned empirical formula in the region of excitation energy $E^* < 30$ MeV. Including these effects of vibrational and rotational enhancements, the final total NLD is given as [25,29]

$$\tilde{\rho}(E^*) = k_{\text{rot}} k_{\text{vib}} \omega(E^*)/(\sigma_\parallel \sqrt{2\pi}). \qquad (14)$$

By using the nuclear temperature $\tilde{T}(E) = [\partial \ln \tilde{\rho}(E)/\partial E]^{-1}$, which is defined from Eqs. (1) and (14), one finds from Eq. (2) the parameter $B(\tilde{T})$ simply as

$$B(\tilde{T}) = \tilde{\rho}(E^*) e^{-E^*/\tilde{T}}. \qquad (15)$$

III. ANALYSIS OF THE NUMERICAL RESULTS

The numerical calculations are carried out for $^{60-62}$Ni and $^{170-172}$Yb isotopes, whose single-particle spectra are taken from the axially deformed Woods-Saxon potentials, following

the method described in Ref. [30]. By defining the nuclear shape in terms of a multipole expansion into spherical harmonics, this method diagonalizes a model Hamiltonian including the spin-orbit interaction and Coulomb potential for protons in the axially deformed harmonic-oscillator basis, which allows up to 19 harmonic-oscillator shells. The single-particle spectra used in the present calculations span a large space from the bottom of the potential up to the major shell with $N = 126$ (five harmonic-oscillator shells). The neutron spectra are from around -39 and -40 MeV up to around 25 and 10 MeV, whereas the proton spectra are from around -34 and -33 MeV up to 30 and 19 MeV for Ni and Yb isotopes, respectively. The distances $\epsilon_p^{\max} - \epsilon_h^{\min}$ between the highest particle (p) state (top) and lowest hole (h) state (bottom) of these spectra amount to 64 and 50 MeV for neutrons, whereas for protons they are 64 and 52 MeV for Ni and Yb isotopes, respectively, which well cover the regions of giant dipole resonances. The values of the quadrupole deformation parameter β_2 obtained
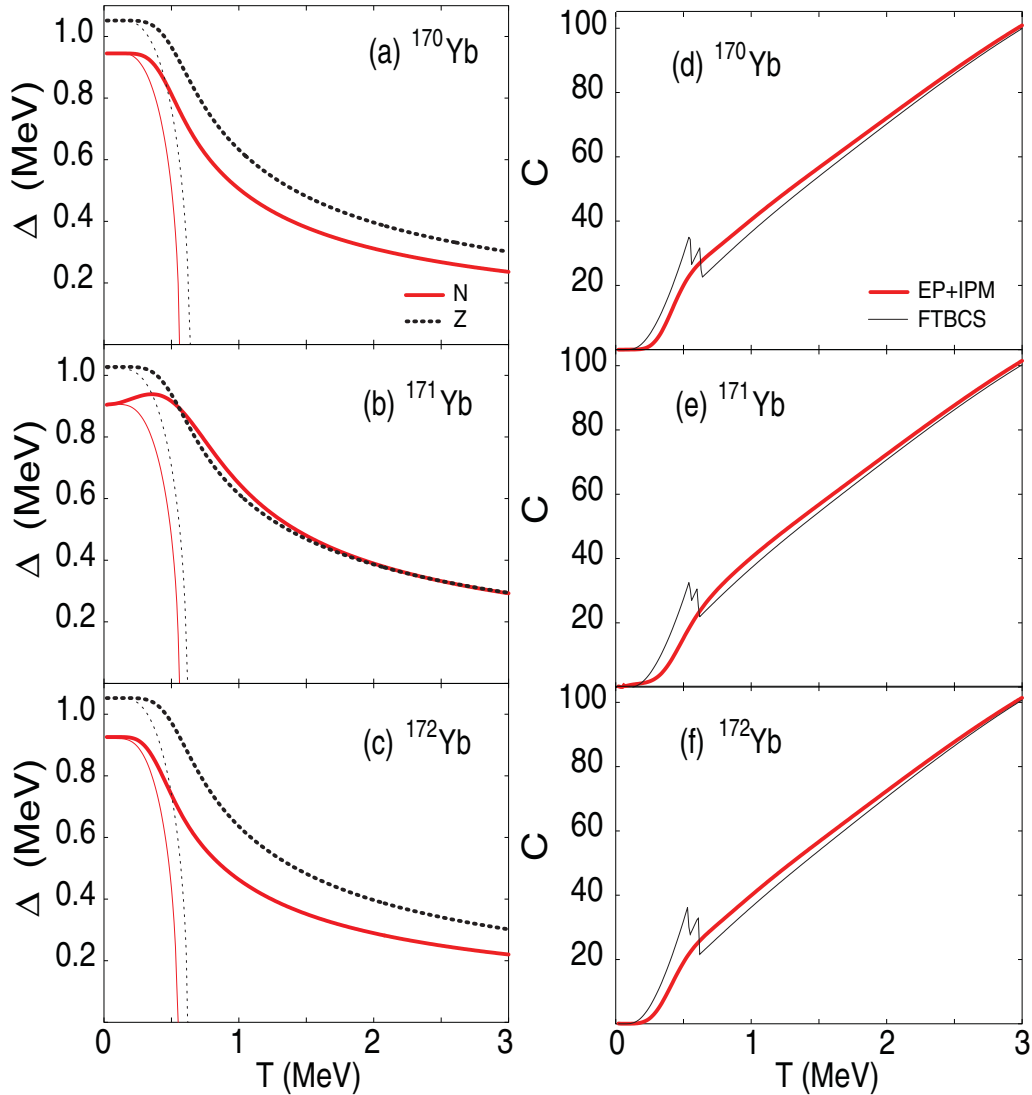
FIG. 2. The same as in Fig. 1 but for Yb isotopes. The thick and thin lines stand for the EP + IPM and FTBCS results, respectively.

from the mass calculations in Ref. [31] are employed. They are estimated from the experimental values of the quadrupole transition probability $B(E2; 2_1^+ \rightarrow 0_1^+)$ from the 2_1^+ state to the 0_1^+ one or the experimental binding energy. For $^{60-62}$Ni the values of β_2 are determined as $\beta_2 = 0, -0.13$, and -0.2, respectively, whereas for ^{170,171}Yb and ^{172}Yb these values are determined as 0.295 and 0.296, respectively. The other parameters of the Woods-Saxon potential are the same as those reported in Ref. [30]. The values of the pairing interaction parameter G for neutrons and protons are chosen so that the exact neutron and proton pairing gaps obtained at $T = 0$ reproduce the corresponding experimental values extracted from the odd-even mass differences [32]. For $^{60-62}$Ni isotopes, which are proton closed-shell nuclei ($Z = 28$) ($\Delta_Z = 0$), only neutron pairing is treated by using the values of G_N chosen to be 0.475, 0.48, and 0.473 MeV, respectively. For $^{170-172}$Yb these values are $G_N(G_Z) = 0.25 (0.29), 0.284 (0.286)$, and 0.24 (0.29) MeV, respectively. The diagonalization of the pairing Hamiltonian is carried out for 12 doubly degenerate single-particle levels with six levels above and six levels below

the Fermi surface. A set of a total of 73 789 (69 576) eigenstates for the even (odd) particle number of each type of particles is obtained and employed to construct the exact CE partition function. The remaining portion of the single-particle spectrum outside this truncated space is treated within the IPM as has been discussed in the previous section.

Shown in Figs. 1(a)–1(c) are the results of the exact (the thick lines) and the FTBCS (the thin lines) neutron gaps as functions of T in $^{60-62}$Ni isotopes. The exact pairing gap is defined following Eq. (18) in Ref. [16]. Although the FTBCS gaps collapse at the critical temperatures of $T_c = 0.99$ MeV for ^{60,62}Ni and 0.85 MeV for ^{61}Ni, the exact gaps generally decrease with increasing T and remain finite well above T_c. Even at $T = 3$ MeV their values are still as large as around 0.7 MeV. In ^{61}Ni a slight increase in the gap is observed at $T < 1$ MeV because of the decrease in the blocking effect from the odd neutron [33]. The heat capacities obtained within the FTBCS show a prominent spike at T_c as the manifestation of the phase transition from the superfluid phase to the normal one, whereas the exact heat capacities only have a small bump
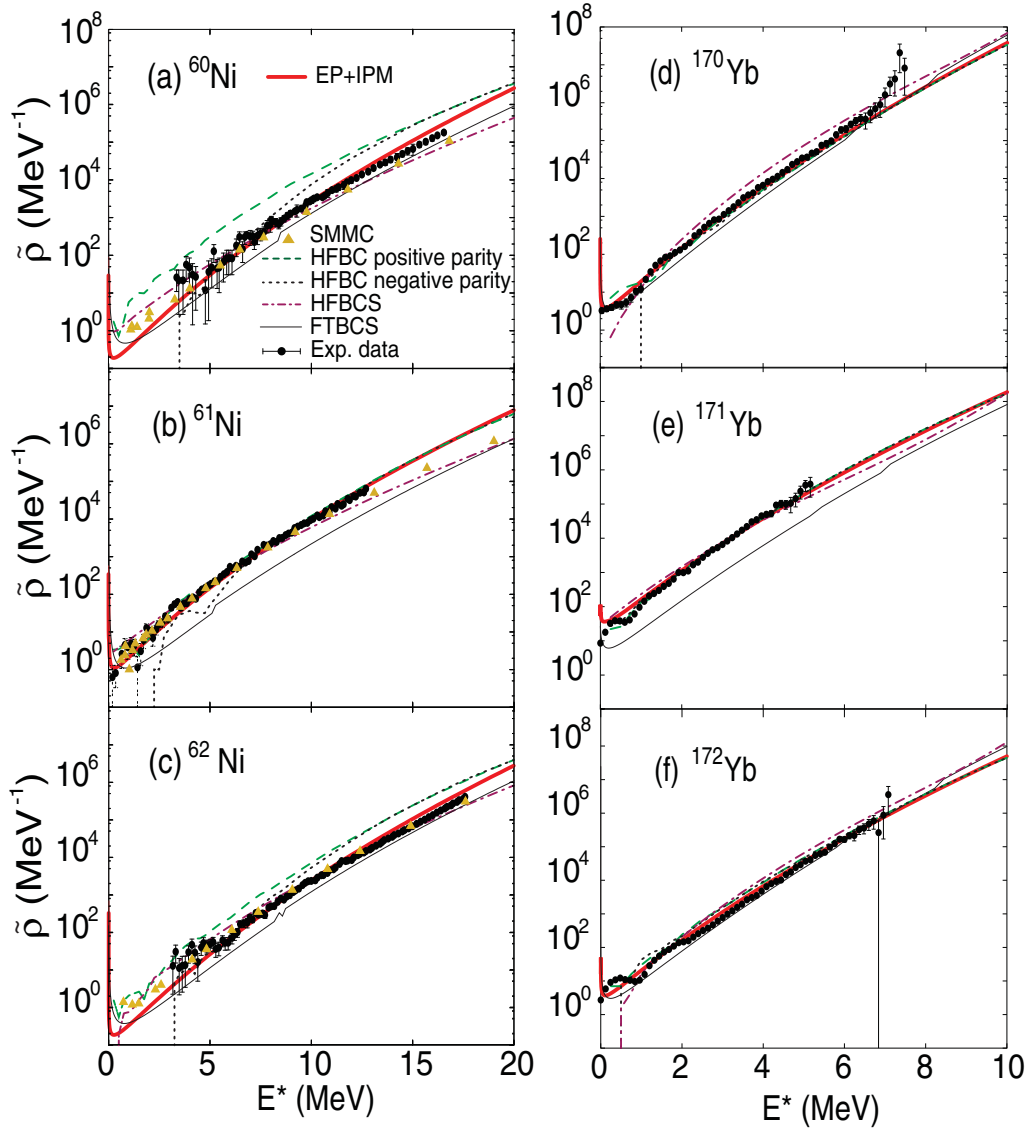
FIG. 3. Total level densities ρ as functions of E^* obtained within the EP + IPM (the thick solid line) and the FTBCS (the thin solid line) in comparison with predictions of SMMC calculations (the triangles) [(a)–(c)], the HFBC calculations for the positive (the dashed lines) and negative parities (the dotted lines), and the HFBCS ones (the dashed-dotted lines). The experimental data for Ni and Yb isotopes are from Refs. [34,38,39], resepctively.

in the region around T_c, confirming that the phase transition is smoothed out [Figs. 1(d)–1(f)]. The increase in the heat capacities with T at high T also assures that the single-particle spectra employed in the calculations are sufficiently large.

Similar features are seen for Yb isotopes where the FTBCS heat capacities have two peaks located at T_c [Figs. 2(d)–2(f)], which correspond to the collapse of the neutron and proton pairing gaps [Figs. 2(a)–2(c)], whereas the exact results yield smooth curves, which monotonically decrease (the pairing gaps) or increase (the heat capacities) as increasing T.

The NLDs obtained within the EP + IPM (the solid lines) for Ni isotopes and shown in Figs. 3(a)–3(c) as functions of E^* agree much better with the experimental data [34] than the predictions by the global microscopic calculations within the HFBC method for both negative (the dashed lines)

and positive (the dotted lines) parities, whose values are taken from the RIPL-3 database [35]. The latter noticeably overestimate experimental NLDs for ^{60,62}Ni. The source of this discrepancy comes from the fact that, to have a good description of the experimental data, the NLDs obtained within the HFBC method have to be renormalized based on two phenomenological parameters, whose values are extracted from the experimental analysis of the cumulative number of levels and the neutron resonance spacing at the neutron binding energy. Given the absence of these experimental data for $^{60-62}$Ni, the present HFBC results for them are unrenormalized. Regarding the EP + IPM, its exact CE partition function is obtained from the direct diagonalization of the matrix elements of the pairing Hamiltonian (3), including all possible couplings among the ph, pp, and hh states without the necessity of any renormalization of the NLDs. As compared to the prediction
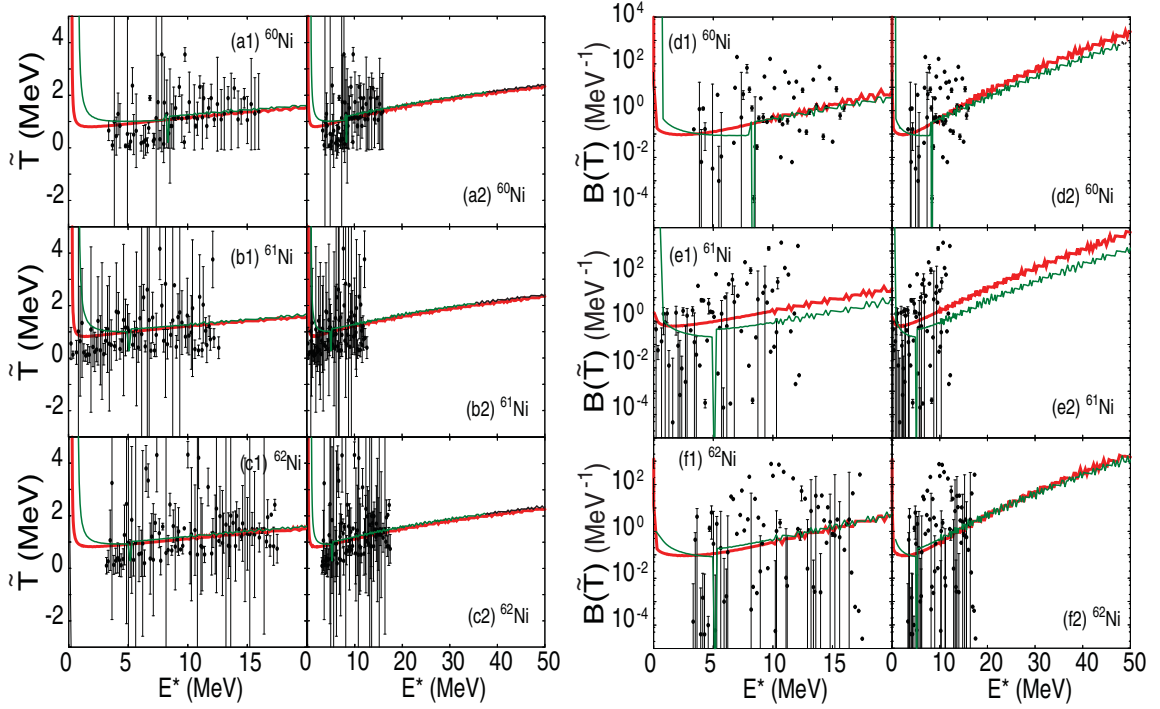
FIG. 4. Nuclear temperature $\tilde{T}$, calculated from Eq. (1) by using the NLD $\tilde{\rho}(E^*)$ (14) and parameter $B(\tilde{T})$ (15) as functions of excitation energy E^* for $^{60-62}$Ni isotopes (the thick solid lines). The corresponding results obtained within the FTBCS are shown by the thin solid lines. The data points are obtained by using the experimental NLDs from Ref. [34].

by the Hartree-Fock plus BCS (HFBCS) approach [36], the EP + IPM results in general have a steeper slope, which is lower at $E^* \leqslant 7$–7.7 MeV (10 MeV) for ^{60,61}Ni (^{62}Ni) and slightly higher at larger E^* than that obtained within the

HFBCS. In the low-E^* region the predictions by both the EP + IPM and the HFBCS agree well with the experimental data (within the experimental error bars). In the high-E^* region the EP + IPM results still are closer to the experimental data
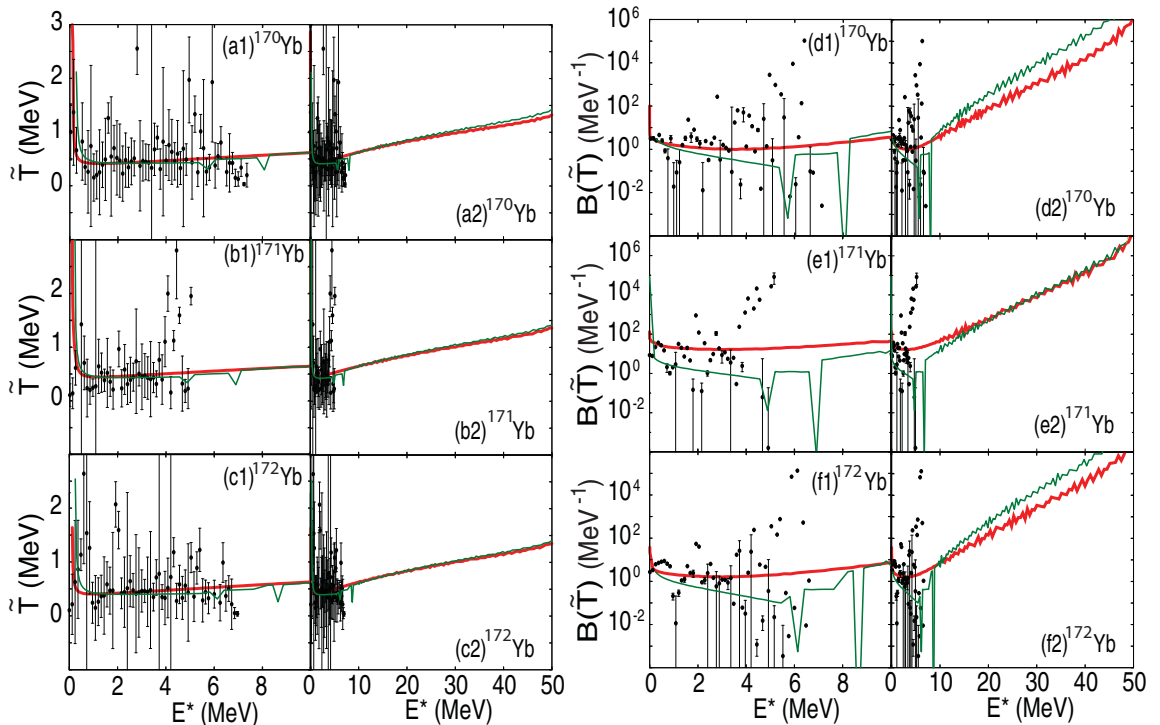

FIG. 5. The same as in Fig. 4 but for $^{170-172}$Yb isotopes. The data points are obtained by using the experimental NLDs from Refs. [38,39].
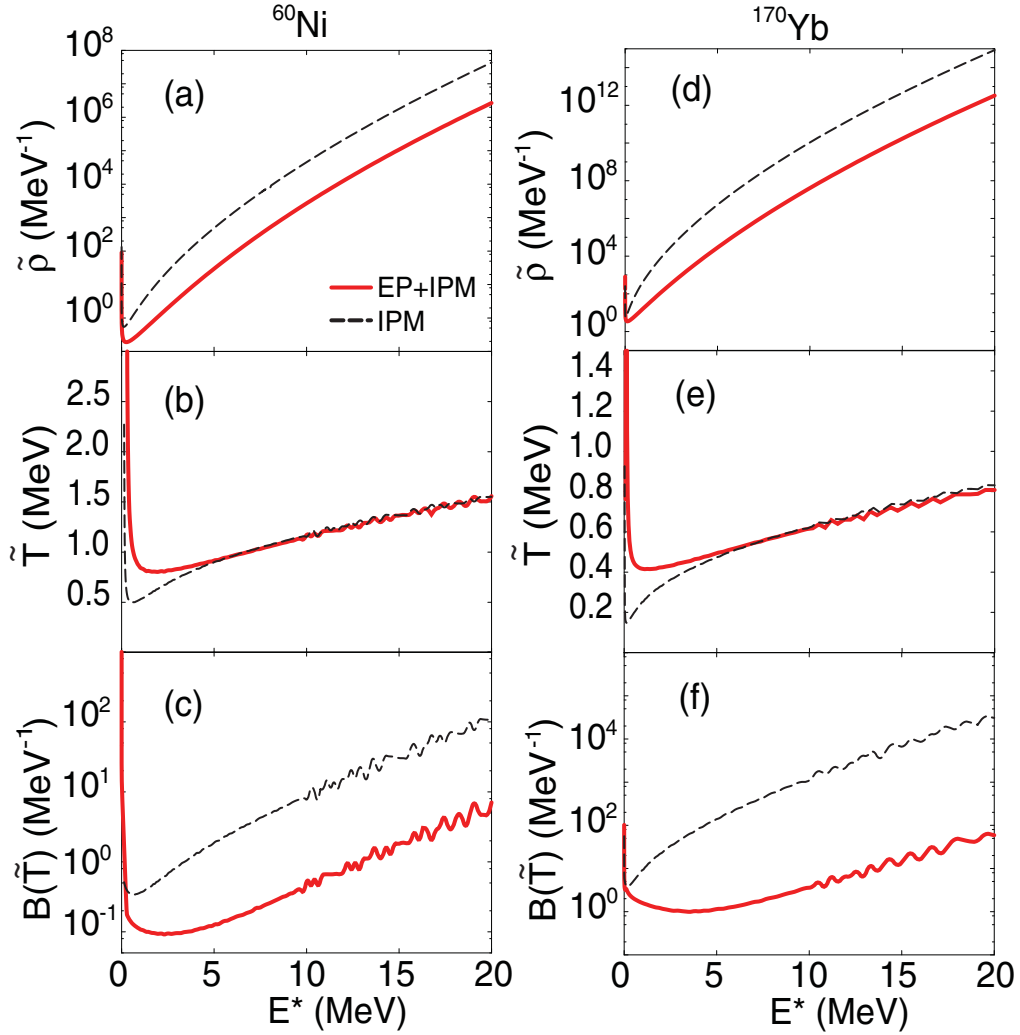
FIG. 6. Comparison of NLD $\tilde{\rho}$ (14), temperature $\tilde{T}$, which is calculated from Eq. (1) by using $\tilde{\rho}$, and coefficient $B(\tilde{T})$ (15) for ^{60}Ni and ^{170}Yb (the solid lines) with their corresponding values obtained without pairing (the dashed lines).

than the HFBCS ones especially for ^{60,61}Ni. The prediction by the shell-model Monte Carlo (SMMC) approach [37] is bracketed between the EP + IPM and the HFBCS results in the low-E^* region but closer to the HFBCS one at high E^*.

For Yb isotopes, the total NLDs obtained within the EP + IPM and HFBC (after being renormalized) and shown in Figs. 3(d)–3(f) agree quite well with the experimental data and generally better than the predictions by the HFBCS. The latter overestimates the experimental data for ^{170,172}Yb at $E^* > 2$ MeV. For ^{171}Yb the HFBCS slightly overestimates the experimental NLD at $0.5 < E^* < 2$ MeV and underestimates it at $E^* > 5$ MeV. Meanwhile, the FTBCS in general underestimates the experimental data, in particular, for the odd isotopes ^{61}Ni and ^{171}Yb.

The nuclear temperature $\tilde{T}$, which was calculated by using the definition (1) and the total NLD $\tilde{\rho}(E^*)$ in Eq. (14) for $^{60-62}$Ni isotopes, is displayed in Figs. 4(a1)–4(c2) as a function of E^* from which panels (a1), (b1), and (c1) are the portions at low excitation energy ($E^* \leqslant 20$ MeV) of the corresponding panels on their right, that is, (a2), (b2), and (c2).

The corresponding values of the parameter $B(\tilde{T})$, which were calculated by using Eq. (15), are plotted in Figs. 4(d1)–4(f2). The data points are obtained by using the same Eqs. (1) and (15) but with the experimental NLDs from Ref. [34] instead of $\tilde{\rho}(E^*)$ (14). The results in Figs. 4(a1)–4(c2) show that, except for the region of very low excitation energy below 1 MeV, the nuclear temperature $\tilde{T}$ increases almost linearly with E^* but this increase is relatively slow so that $\tilde{T}$ can be approximated with a constant of around 1–1.5 MeV at E^* within the energy interval where the data points are available. The values of $\tilde{T}_{\text{FTBCS}}$ and $B(\tilde{T})_{\text{FTBCS}}$, which are obtained by using $\tilde{\rho}(E^*)_{\text{FTBCS}}$ calculated within the FTBCS, also are shown in Figs. 4(a1)–4(f2) for comparison (the thin solid lines). At $E^* \geqslant 5$ MeV, the thin line, which describes the dependence of $\tilde{T}_{\text{FTBCS}}$ on E^*, almost coincides with the thick line for $\tilde{T}$ obtained within the EP + IPM except at E_c^* corresponding to the critical temperature T_c where the FTBCS pairing gap collapses. As for $B(\tilde{T})_{\text{FTBCS}}$, it undergoes not only a singularity in the form of a deep minimum, but also a jump at E_c^*, below (above) which $B(\tilde{T})_{\text{FTBCS}}$ decreases (increases) with increasing E^*.

A quite similar feature is also seen in $^{170-172}$Yb isotopes as displayed in Fig. 5 where the data points were obtained by using the experimental NLDs from Refs. [38,39]. This figure also shows that the temperature $\tilde{T}$ remains nearly constant at around 0.5 MeV between $E^* \simeq 0.4$ and 0.6 MeV up to $E^* \simeq 10$ MeV, that is, within the original assumption on the validity of the CT model. The E^* dependences of $\tilde{T}_{\text{FTBCS}}$ and $B(\tilde{T})_{\text{FTBCS}}$ now have two singular points, corresponding to the collapse of the FTBCS neutron and proton pairing gaps, below which $B(\tilde{T})_{\text{FTBCS}}$ is generally smaller than $B(\tilde{T})$ obtained within the EP + IPM.

It can also be observed from these results that the values of the coefficient $B(\tilde{T})$ obtained in odd-mass isotopes ^{61}Ni and ^{171}Yb are about one order larger than the corresponding values in the neighboring even-even nuclei. The source of this difference is the pairing suppression at low excitation energy in odd-mass nuclei because of the blocking effect [33].

In Fig. 6 we compare the NLDs $\tilde{\rho}(E^*)$, temperature $\tilde{T}$, and coefficient $B(\tilde{T})$ obtained for ^{60}Ni and ^{170}Yb within the EP + IPM (the solid lines) with their corresponding values obtained within the IPM (the dashed lines), that is, without pairing. The figure shows that the slope of the NLDs obtained without pairing [the dashed lines in Figs. 6(a) and 6(d)] is steeper than that of the results obtained with exact pairing. Consequently, the dependence of $\tilde{T}$ on the excitation energy E^* is depleted at $E^* < 5$ MeV [the dashed lines in Figs. 6(b) and 6(e)], worsening the validity of the CT model in this region of low excitation energy. The corresponding values of the coefficient $B(\tilde{T})$ become larger by around one and two orders at $E^* > 5$ MeV for ^{60}Ni and ^{170}Yb, respectively. The slope of $B(\tilde{T})$ obtained without pairing also gets steeper at $E^* < 5$ MeV. At $E^* > 5$ MeV, pairing has almost no effect on $\tilde{T}$ because the lines describing the E^* dependences of the NLDs obtained by using exact pairing [the thick lines in Figs. 3, 6(a), and 6(d)], FTBCS pairing (the thin lines in Fig. 3), and without pairing [the dashed lines in Figs. 6(a) and 6(d)] are almost parallel to each other. This makes their derivatives over E^* almost identical, so are the values of $\tilde{T}$ defined from Eq. (1).

The arithmetic means $\langle \tilde{T} \rangle$ of temperatures $\tilde{T}$ and $\langle B(\tilde{T}) \rangle$ of the coefficients $B(\tilde{T})$ within the intervals of excitation energy $E_i^* \leqslant E^* \leqslant E_f^*$ with $E_i^* = 1$, $E_f^* = 20$, and 10 MeV for nickel and ytterbium isotopes, respectively, are collected in Table I. For ^{60}Ni the arithmetic mean $\langle \tilde{T} \rangle = 1.11$ MeV is slightly lower than the value found in Ref. [34] where it has been shown that the NLDs in ^{60}Ni and ^{60}Co can be quite well described by the CT model at a constant temperature of $T = 1.4$ MeV up to $E^* = 20$ MeV. Nonetheless, this value of temperature still is located well between $T_i = 0.84$ and $T_f = 1.52$ MeV obtained at $E_i^* = 1$ and $E_f^* = 20$ MeV, respectively.

The choice of $\tilde{T} = 1.4$ MeV, proposed in Ref. [34], does not seem to be unique because any value of $\tilde{T}$ within the energy interval $1\,\text{MeV} < E^* \leqslant 20$ MeV, which is obtained from the same NLD $\tilde{\rho}(E^*)$ (14), whose corresponding to a coefficient $B(\tilde{T})$ remains approximately constant within this energy interval, can serve as an alternative. To demonstrate this, in Fig. 7(b), we show the coefficient $B(\tilde{T})$ obtained at several temperatures [Fig. 7(a)] to reproduce the NLD $\tilde{\rho}(E^*)$

TABLE I. Arithmetic means $\langle \tilde{T} \rangle$ of temperatures $\tilde{T}$ and $\langle B(\tilde{T}) \rangle$ of the coefficient $B(\tilde{T})$ in the energy interval $E_i^* \leqslant E^* \leqslant E_f^*$ with $E_i^* = 1$ MeV, whereas $E_f^* = 20$ MeV for $^{60-62}$Ni and 10 MeV $^{170-172}$Yb isotopes. The values of $\tilde{T}_i$ at E_i^* and $\tilde{T}_f$ at E_f^* as well as the corresponding values $B_i \equiv B(\tilde{T}_i)$ and $B_f \equiv B(\tilde{T}_f)$ of coefficient $B(\tilde{T})$ (15) also are shown.

Nucleus	$\tilde{T}$ (MeV)		$B(\tilde{T})$ (MeV^{-1})		Arithmetic mean	
	$\tilde{T}_i$	$\tilde{T}_f$	B_i	B_f	$\langle \tilde{T} \rangle$	$\langle B(\tilde{T}) \rangle$
^{60}Ni	0.84	1.52	0.11	6.04	1.11	1.02
^{61}Ni	0.84	1.54	0.64	20.5	1.14	4.38
^{62}Ni	0.89	1.53	0.11	5.03	1.09	0.79
^{170}Yb	0.41	0.61	1.51	3.62	0.50	1.55
^{171}Yb	0.45	0.65	20.5	41.6	0.53	22.5
^{172}Yb	0.41	0.64	2.02	7.46	0.50	2.72

in ^{60}Ni within the energy interval $0 < E^* \leqslant 20$ MeV. As seen in Fig. 7(b), the lines showing the dependence of $B(\tilde{T})$ on E^* obtained at $\tilde{T} = 1.3$, 1.4, and 1.52 MeV weakly change with E^* in the interval $5\,\text{MeV} \leqslant E^* \leqslant 20$ MeV so that they can be approximated by corresponding constant values.

Shown in Fig. 8 are the predictions for the NLD $\rho(E^*)$ in ^{60}Ni by the CT model (2) at $T = 1.3$, 1.4, and 1.5 MeV for which the corresponding constant (E^*-independent) values of the coefficient B are found so that the best fit to the experimental NLDs is achieved. As compared to the prediction
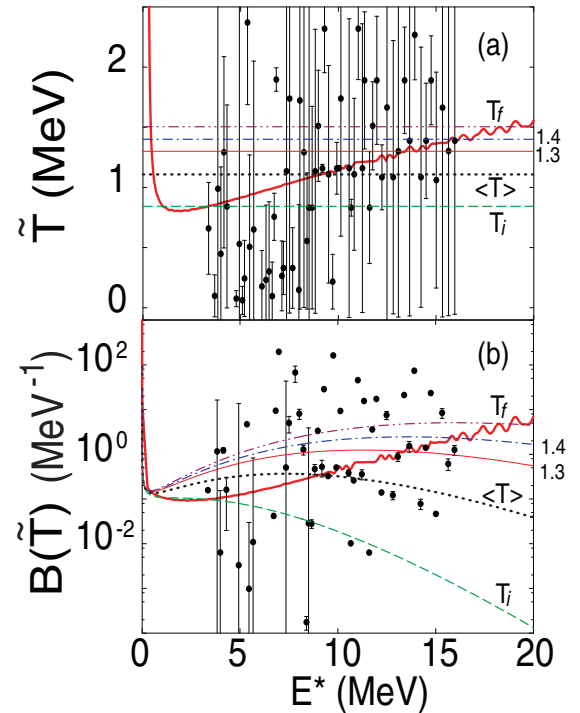

FIG. 7. Coefficient $B(\tilde{T})$ (15) (b) obtained at several temperatures, $\tilde{T} = T_i$ (0.84 MeV), $\langle T \rangle$ (1.11 MeV), 1.3, 1.4 MeV, and T_f (1.52 MeV) [the horizontal lines in (a)] from the NLD $\tilde{\rho}(E^*)$ in ^{60}Ni as functions of excitation energy E^*.
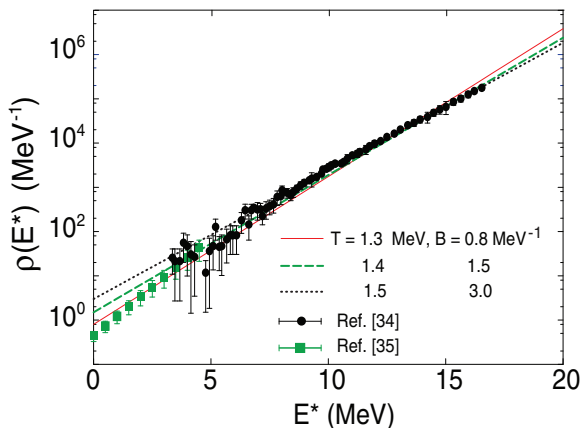
FIG. 8. Comparison of NLDs $\rho(E^*)$ obtained from the CT model (2) at $T = 1.3$ (the solid line), 1.4 (the dashed line), and 1.5 (the dotted line) MeV and experimental NLDs for ^{60}Ni.

with $T = 1.4$ MeV and $B = 1.5$ MeV^{-1}, the NLD obtained with $T = 1.3$ MeV and $B = 0.8$ MeV^{-1} gives a better fit to the low-energy data [35]. The latter were extracted from the analysis of the experimental level scheme within the interval $0 \leqslant E^* \leqslant 4.613$ MeV with $T = 0.9836 \pm 0.0952$ and $E_0 = 0.8242 \pm 0.2981$ MeV, which corresponds to a value of $B = 0.44^{+0.18}_{-0.11}$ MeV^{-1} in Eq. (2). The NLD obtained with $T = 1.5$ MeV and $B = 3.0$ MeV^{-1} agrees slightly better with the data in the region 10 MeV $\leqslant E^* \leqslant 20$ MeV. However, all three predictions overall agree with the experimental data within the whole interval $0 < E^* \leqslant 20$ MeV. In other words, one may say that, for ^{60}Ni, the CT model of the NLD is valid up to $E^* = 20$ MeV with any constant value of temperature within the interval $1.3 \leqslant T \leqslant 1.5$ MeV.

IV. CONCLUSIONS

In the present paper, by using the NLD predicted within the EP + IPM method, which agrees well with the experimental data, the nuclear temperature $\tilde{T}$ is calculated from the derivative of the logarithm of NLD (1). This temperature $\tilde{T}$ increases almost linearly with the excitation energy E^*. However this increase is relatively slow so that $\tilde{T}$ can be considered as a constant of around 0.5 MeV at $0 < E^* \leqslant 10$ MeV for ytterbium isotopes. Meanwhile, in ^{60}Ni, the CT model can describe rather well the experimentally extracted NLD with a constant temperature between $1.3 \leqslant \tilde{T} \leqslant 1.5$ MeV up to $E^* = 20$ MeV, which is much higher than the particle separation threshold. This feature is in excellent agreement with the experimental finding of Ref. [34]. It is also shown that pairing plays an important role in maintaining this nearly constant value of temperature at low excitation energy. In this way, the EP + IPM offers a consistent description of the NLD, which goes smoothly from the low-energy region $E^* \leqslant 5$ MeV to the higher one (up to 20 MeV for Ni isotopes and 10 MeV for Yb isotopes) without the need for matching the CT model at low energy and the Fermi-gas one at high energy as often performed by using the composite level-density formula [5]. As a matter of fact, the values of the matching energy E_x defined from the composite level-density formula by using Eq. (26) and Table III in Ref. [5] are 7.49, 6.16, and 7.53 MeV for Ni isotopes with $A = 60, 61$, and 62, respectively. For $^{170-172}$Yb they are 4.67, 4.06, and 4.74 MeV, respectively. Last but not least, the fact that the NLD at low excitation energy, even at $E^* = 0$, can be described well by the CT model at a constant nonzero temperature also supports the suggestion of introducing a ground-state's effective temperature [40].

[1] T. Ericson, Adv. Phys. **9**, 425 (1961).

[2] T. Rauscher and F. K. Thielemann, At. Data Nucl. Data Tables **75**, 1 (2000).

[3] T. Rauscher, F. K. Thielemann, and K. L. Kratz, Phys. Rev. C **56**, 1613 (1997).

[4] H. A. Bethe, Phys. Rev. **50**, 332 (1963); Rev. Mod. Phys. **9**, 69 (1937).

[5] A. Gilbert and A. G. W. Cameron, Can. J. Phys. **43**, 1446 (1965).

[6] A. V. Voinov, B. M. Oginni, S. M. Grimes, C. R. Brune, M. Guttormsen, A. C. Larsen, T. N. Massey, A. Schiller, and S. Siem, Phys. Rev. C **79**, 031301(R) (2009).

[7] M. Guttormsen, B. Jurado, J. N. Wilson, M. Aiche, L. A. Bernstein, Q. Ducasse, F. Giacoppo, A. Görgen, F. Gunsing, T. W. Hagen, A. C. Larsen, M. Lebois, B. Leniau, T. Renstrøm, S. J. Rose, S. Siem, T. Tornyi, G. M. Tveten, and M. Wiedeking, Phys. Rev. C **88**, 024307 (2013).

[8] M. Guttormsen, L. A. Bernstein, A. Görgen, B. Jurado, S. Siem, M. Aiche, Q. Ducasse, F. Giacoppo, F. Gunsing, T. W. Hagen, A. C. Larsen, M. Lebois, B. Leniau, T. Renstrøm, S. J. Rose, T. G. Tornyi, G. M. Tveten, M. Wiedeking, and J. N. Wilson, Phys. Rev. C **89**, 014302 (2014).

[9] L. G. Moretto *et al.*, J. Phys.: Conf. Ser. **580**, 012048 (2015).

[10] L. G. Moretto, Phys. Lett. **40B**, 1 (1972).

[11] R. Rossignoli, P. Ring, and N. Dinh Dang, Phys. Lett. B **297**, 9 (1992); N. Dinh Dang, P. Ring, and R. Rossignoli, Phys. Rev. C **47**, 606 (1993).

[12] V. Zelevinsky, B. A. Brown, N. Frazier, and M. Horoi, Phys. Rep. **276**, 85 (1996).

[13] D. J. Dean, S. E. Koonin, K. Langanke, P. B. Radha, and Y. Alhassid, Phys. Rev. Lett. **74**, 2909 (1995).

[14] N. Dinh Dang and A. Arima, Phys. Rev. C **68**, 014318 (2003); N. Dinh Dang and V. Zelevinsky, *ibid.* **64**, 064319 (2001); N. Dinh Dang, Nucl. Phys. **A784**, 147 (2007).

[15] N. Dinh Dang and N. Quang Hung, Phys. Rev. C **77**, 064315 (2008).

[16] N. Quang Hung and N. Dinh Dang, Phys. Rev. C **79**, 054328 (2009).

[17] R. Sen'kov and V. Zelevinsky, Phys. Rev. C **93**, 064304 (2016).

[18] N. Quang Hung, N. Dinh Dang, and L. T. Quynh Huong, Phys. Rev. Lett. **118**, 022502 (2017).

[19] A. Volya, B. A. Brown, and V. Zelevinsky, Phys. Lett. B **509**, 37 (2001).

[20] N. Quang Hung and N. Dinh Dang, Phys. Rev. C **81**, 057302 (2010).

[21] N. Quang Hung and N. Dinh Dang, Phys. Rev. C **82**, 044316 (2010).

[22] Y. Alhassid, G. F. Bertsch, and L. Fang, Phys. Rev. C **68**, 044322 (2003).

[23] H. Nakada and Y. Alhassid, Phys. Rev. Lett. **79**, 2939 (1997).

[24] W. Dilg, W. Schantl, H. Vonach, and M. Uhl, Nucl. Phys. **A217**, 269 (1973).

[25] A. R. Junghans *et al.*, Nucl. Phys. **A629**, 635 (1998); M. N. Nasrabadi and M. Sepiani, Acta Phys. Pol., B **45**, 1865 (2014).

[26] A. V. Ignatyuk, *The Statistical Properties of the Excited Atomic Nuclei* (Energoatomizdat, Moscow, 1983); S. Bjørnholm, A. Bohr, and B. Mottelson, *Proceedings of the Symposium on Physics and Chemistry of Fission* (IAEA, Vienna, 1974), Vol. I, p. 367.

[27] A. S. Iljinov, Nucl. Phys. **A543**, 517 (1992).

[28] S. Goriely, S. Hilaire, and A. J. Koning, Phys. Rev. C **78**, 064307 (2008).

[29] R. Capote *et al.*, Nucl. Data Sheets **110**, 3107 (2009).

[30] S. Cwiok, J. Dudek, W. Nazarewicz, J. Skalski, and T. Werner, Comput. Phys. Commun. **46**, 379 (1987).

[31] P. Möller, J. R. Nix, W. D. Myers, and W. J. Swiatecki, Atomic Data Nucl. Data Tables **59**, 185 (1995).

[32] N. Zeldes, A. Grill, and A. Siemievic, Mat. Fys. Skr. Dan. Vid. Selsk. **3**, 5 (1967); A. Bohr and B. Mottelson, *Nuclear Structure* (Benjamin, NY, 1969), Vol. 1, p. 170.

[33] N. Quang Hung, N. Dinh Dang, and L. T. Quynh Huong, Phys. Rev. C **94**, 024341 (2016).

[34] A. V. Voinov, S. M. Grimes, C. R. Brunes, T. Massey, and A. Schiller, EPJ Web Conf. **21**, 05001 (2102).

[35] https://www-nds.iaea.org/RIPL-3/

[36] P. Demetriou and S. Goriely, Nucl. Phys. **A695**, 95 (2001).

[37] M. Bonett-Matiz, A. Mukherjee, and Y. Alhassid, Phys. Rev. C **88**, 011302(R) (2013).

[38] A. Schiller, A. Bjerve, M. Guttormsen, M. Hjorth-Jensen, F. Ingebretsen, E. Melby, S. Messelt, J. Rekstad, S. Siem, and S. W. Ødegård, Phys. Rev. C **63**, 021306(R) (2001).

[39] U. Agvaanluvsan, A. Schiller, J. A. Becker, L. A. Bernstein, P. E. Garrett, M. Guttormsen, G. E. Mitchell, J. Rekstad, S. Siem, A. Voinov, and W. Younes, Phys. Rev. C **70**, 054611 (2004).

[40] V. Zelevinsky, *12th International Spring Seminar on Nuclear Physics Current Problems and Prospects for Nuclear Structure Sant'Angelo d'Ischia, 2017* (INFN, Naples, 2017).